Nanocomposite MFI – ceramic hollow fibres: prospects for CO_2 separation

A. Alshebani[1], M. Pera-Titus[1], E. Landrivon[1], Th. Schiestel[2], S. Miachon[1,*] and J.-A. Dalmon[1]

[1]*Institut de Recherches sur la Catalyse et l'Environnement de Lyon (IRCELYON), UMR 5256 CNRS - Université Claude Bernard Lyon 1, 2, av. A. Einstein, 69626 Villeurbanne cedex, France*

[2] *Fraunhofer Institute for Interfacial Engineering and Biotechnology, Inorganic Surfaces and Membranes, Nobelstrasse 12, 70569 Stuttgart, Germany*

* to whom correspondence should be addressed at Sylvain.Miachon@ircelyon.univ-lyon1.fr

Abstract

The membrane surface / module volume ratio is one of the main criterion in designing separation units. This parameter can be increased by one order of magnitude when dropping the membrane tube diameter from the cm to the mm scale. Alumina hollow fibres have been used as supports and submitted to pore-plugging MFI zeolite synthesis. An alumina-MFI nanocomposite structure, showing no surface film, has been obtained, as observed by SEM and EDX analysis and confirmed by high temperature variation of H_2 and N_2 permeances. Maxwell-Stefan modeling provides an equivalent thickness lower than 1 µm. The membrane quality has been assessed by gas separation of n-butane/H_2. A first application to CO_2/H_2 separation has been achieved, reaching separation factors close to 10. Such a system, based on cheap symmetric supports, could lead to an important decrease in module costs for gas separation applications.

Keywords: MFI membrane, nanocomposite, hollow fibre, CO_2.

1. Introduction

The use of hollow fibre geometry has long been a solution to improve the performance of membrane-based separation processes. In liquid phase (e.g., water treatment), polymer hollow fibres are commonly used at the industrial scale. Similarly, in gas separation, they are widely used in refinery or ammonia production industries for instance. Low cost, associated with large surface / volume ratios (>1000 $m^2 \cdot m^{-3}$), make them the configuration of choice for a large number of membrane-based applications.

Until now, most zeolite membranes have been implemented in single tubes, multichannel tubes and monoliths or planar geometries. Some zeolite – polymer mixed matrix materials have also been described in hollow fibre form [1], showing some gas permselectivity, but permeances in the order of $nmol \cdot m^{-2} \cdot s^{-1} \cdot Pa^{-1}$, typical of polymer membranes. Other works have been reported on purely inorganic materials. Smith et al. [2] have shown the preparation of zeolite membranes based on carbon hollow fibres, but with neither permeation nor separation tests. More recently, Richter et al. [3] published a work based on 'capillaries' (i.e. tubes of about 4 mm diameter), with single gas permeances around 0.5 $\mu mol \cdot m^{-2} \cdot s^{-1} \cdot Pa^{-1}$, but no quality testing was provided further, making it very difficult to assess for membrane quality. Moreover, this work keeps the idea of using asymmetric supports. Finally, the structure shown in that work remains a relatively thick film-like structure (30 μm). Xu et al. [4] presented the synthesis of zeolite NaA membranes on 0.4 mm diameter ceramic hollow fibres, showing a continuous 5-μm film offering typical single permeances of ~0.03 $\mu mol \cdot m^{-2} \cdot s^{-1} \cdot Pa^{-1}$. Membrane quality was estimated by pure gas permeance only, which is difficult to use for reliable defect searching [5].

In the present work, we propose to use hollow fibres to apply the concept of nanocomposite structure proposed by our group in recent works for MFI/ceramic membranes [6-8]. Nanocomposite MFI/ceramic fibres might offer several advantages compared to conventional film-like zeolite membranes. In the nanocomposite architecture, the active phase is not made of a film on the top of a porous support, but rather embedded into the support pores via pore-plugging synthesis. This not only allows individual membrane defects not to exceed the size of the support pores, but also provides a better mechanical resistance, as well as a higher resistance to thermal shocks. Moreover, the thermal behaviour of nanocomposite membranes prepared so far differs from their film-like counterparts [5,8].

The characteristics mentioned above, all eventually translating into cost for the final application, make nanocomposite MFI/ceramic fibres ideal candidates for carbon dioxide separation, for which MFI has shown to be permselective in certain conditions [9]. The supports here used (1.7 mm diameter) are larger than common polymeric hollow fibres. However, ceramic membranes show higher permeance together with higher thermal and mechanical stability. Moreover, in the present case, the cost of the starting support, because of its symmetrical structure, would not be a limiting factor.

Due to its asserted role in the global climate change, the separation of carbon dioxide from gas emissions is one of the main challenges of membrane researchers and manufacturers at present. Therefore, this molecule has been chosen as a target for the zeolite hollow fibre development. As a matter of fact, this application in the future will require highly compact systems.

2. Experimental

2.1. Ceramic support

Ceramic hollow fibres were manufactured by a wet spinning process [10]. Alumina particles (SUMITOMO α-Al_2O_3, mean particle size: 0.33 μm) were mixed with a solution of Polysulfone (SOLVAY UDEL P-3500) in N-Methylpyrrolidone (MERCK) and were ball-milled for 16 h. This slurry was spun through a spinneret into a water bath where the polymer precipitated incorporating the ceramic particles. The resulting green fibres were cut into 30-cm pieces and sintered to full ceramic hollow fibres. The properties of the final fibres are summarized in Table 1.

Table 1.
Properties of the ceramic hollow fibres used as supports for zeolite membrane synthesis in this work

Mean outer diameter	1.65 mm
Mean wall thickness	230 μm
Mechanical stability (3-point bending test)	112 MPa
Porosity	43%
First bubble point	2.5 bara

The support quality was tested using a method based on gas-liquid displacement. In this method, the porous fibres, after careful sealing on a metal connector using epoxy resin, were first immersed in ethanol to allow the liquid fill up all the porosity. This method consists first of bubble point pressure test by applying an increasing pressure to inside the tube in dead-end mode. According to Laplace Law, the pressure of the first bubble allows the determination of the largest pore size of the fibres. The further increase of the permeating gas flux with the gas overpressure (up to 4 bar by 5 min with 0.5 to 1-bar steps) allowed a relative comparison of fibres of similar structure, with regards to the importance of subsequent smaller defects in the fibres. These measurements were compared to those obtained on conventional 10-mm diameter multilayer tubes used in previous studies. Further details on this method can be found in ref. [6]. Hereinafter this test will be referred to as ‘bubble flow measurement’.

2.2. Zeolite synthesis

The structure directing agent (SDA, 1 M tetrapropylammonium hydroxide, TPAOH, from Aldrich), and the silica source Aerosil 380 (Degussa) were mixed and slightly diluted in deionised water to form a clear solution of molar composition 1.0 SiO_2 : 0.45 TPAOH : 27.8 H_2O (pH close to 14) before a 3-day maturation period at room temperature under stirring.

In order to keep the conditions as close as possible to previous preparations on conventional tubes [5,6], nine 23-cm long ceramic hollow fibres were then inserted into a Teflon®-lined autoclave containing about 25 mL of precursor solution, and submitted to an interrupted hydrothermal synthesis at 423 K for 4 days. Let us underline that the amount of precursor was calculated on the bases of previous work on single tubes considering the ratios precursor volume / porous volume / membrane surface.

The fibres were then washed and dried at 373 K for 12 h. Before calcination at 773 K in air for 4 h, a single N_2 permeation test showed no gas permeance (i.e. below the detection limit of about 10^{-10} mol·m^{-2}·s^{-1}·Pa^{-1}). More details dealing with this one cycle zeolite hydrothermal synthesis and the calcination protocol can be found in refs. [5,6].

2.3. Physical characterisations

The chemical composition of the fibres before and after synthesis was determined by Inductively Coupling Plasma (ICP) elemental analysis (Activa Jobin Yvon) with previous dissolution in 20 wt.% HCl.

The structure of the synthesised zeolite material was analysed by X-ray diffraction (XRD) using a Philips PW1050/81 diffractometer (Cu Kα1+2 radiation). The analyses were performed on powders obtained from crushed fibres before and after hydrothermal synthesis.

Mercury intrusive porosimetry was used to estimate the reduction of macroporosity of the support after hydrothermal synthesis. A Micromeritics Autopore IV 9500 penetrometer was used with samples of 156 mg and 112 mg, respectively, for the fibres before and after zeolite synthesis.

The textural properties of the crushed fibres before and after zeolite synthesis were obtained from N_2 adsorption isotherms at 77 K using a Micromeritics ASAP 2020 sorptometer. BET surface areas were determined from recorded adsorption data in the range $0.30 \leq P/P^o \leq 0.50$.

The morphology of the fibres was inspected by scanning electron microscopy (SEM) using a Hitachi S-800 microscope operating at 10 kV. The samples were obtained by breaking the samples in small pieces. Saw cutting was not used to avoid modifications in the structure during cutting. The local and average Si and Al concentration across the fibres before and after hydrothermal synthesis on the same equipment by energy dispersive X-ray analysis (EDX) using a 1-μm microprobe (Edax Phoenix) with SETW polymer window parallel to the membrane surface.

2.4. *Hollow fibre mounting*

A significant amount of time was devoted to achieving practical mounting and gas sealing of the fibres. As a matter of fact, the sealing should withstand the temperature (i.e. 623 K). Therefore, polymeric sealing was discarded. However, the sealing material had to be processed at temperatures sustainable for the MFI material (i.e. below 1000 K), as the hollow fibres were mounted after hydrothermal synthesis. A home-made glaze, based on a suspension of oxides of aluminium, silicon and sodium in high concentration in water was designed. It was used to immobilize the fibre(s) into a dense alumina tube perforated with small holes, in order to allow easy gas circulation (i.e. sweep gas flow) around the fibre(s), as shown in Fig. 1. This approach is valid for a single fibre (most results shown in this work) and has been extended up to 4 fibres.

This ensemble ‘fibre in tube’ was then mounted in a more conventional membrane stainless steel module initially designed for 10-mm diameter tubular membranes, as described in previous papers [8]. Graphite cylindrical o-rings (Cefilac-Fargraf) were used to seal the support tubes to the module.

Before any transport measurement, the hollow fibres were subjected to an *in situ* high temperature desorption pretreatment at 673 K under 20 NmL·min^{-1} N_2 flow at both sides with a heating ramp of 1 K·min^{-1} for at least 4 h to remove adsorbed species.

Fig. 1. Photographs of 1 and 2 fibres mounted into their mechanical support tube, showing the low temperature glaze fired after hydrothermal synthesis.

2.5. *Single gas permeance*

Single gas (H_2 and N_2) permeance tests were carried out in the temperature range 293-723 K using steady-state steps to assess for the high temperature behaviour of the separative phase and therefore for the nanocomposite structure of the membrane, according to the conclusions derived in a previous study [5]. In these tests, the feed pressure was kept close to 125 kPa and the transfibre pressure ca. 3.2 kPa. A regulating valve at the outlet of the retentate compartment was used to adjust the internal pressure. Another regulating valve at the outlet of the permeate stream was used to control the transfibre pressure difference. More details on the set-up used to carry out gas permeation measurements can be found in a previous paper [8].

In order to evaluation the flux and permeance of the fibre, the surface area used for calculation was obtained using the average diameter of the cylinder (1.53 mm, i.e. 5.5 cm^2 for a 15-cm long fibre).

2.6. *Mixture separation*

Two gas separations were carried out. The room temperature separation of n-butane/H_2 at low temperature was used for quality testing. In such a mixture, the strong adsorption of n-butane in the MFI pores will block H_2 permeation [11]. Therefore, any mesoporous defect in the membrane would locally inverse the selectivity (turning to Knudsen mechanism), and reduce the separation factor. This mixture separation is then more defect-sensitive than other separations [5,6,12]. This separation was carried out further with increasing temperature, in Wicke-Kallenbach mode: the gases were diluted in dry N_2 (15 v/v.%). The feed was kept at about 125 kPa, at a flow rate of 80 Ncm^3/min, with a N_2 counter-current sweep gas of also 80 Ncm^3/min. The transfibre differential pressure was kept at 0.4 kPa.

Moreover, the fibres were also tested for separation of CO_2/H_2 undiluted equimolar mixtures (204 Ncm^3/min feed and 12 Ncm^3/min N_2 sweep, 700 Pa transfibre total pressure) in order to survey a potential application of these materials for CO_2 separation. Keeping equimolar feed, the total feed pressure was varied from 100 to 340 kPa

In both separations, gas flows and feed compositions were controlled by mass-flow controllers (Brooks, type 5850TR and 5850E). A gas chromatograph (HP 5890), using both TCD and FID detectors, was used to measure feed, retentate and permeate compositions. In general terms, the separation factor (Sf) of gas A over gas B (butane over H_2 or CO_2 over H_2) was calculated as the permeate-to-feed composition ratio of the first gas, divided by the same ratio of the second one.

3. Results

3.1. *Quality testing of fibre supports*

In previous studies on tubes, the quality of the support (i.e. the amount and size of larger defects) was shown to be of crucial importance to the final zeolite membrane quality. To this end, prior to hydrothermal synthesis, the fresh fibres were subjected to bubble point tests to assess for the presence of large defects.

Fig. 2 shows a typical bubble flow graph obtained. As can be seen, after a first bubble point (FBP) at 120 kPa (ΔP), comparable to values on tubular supports used in previous studies), a sharp increase is observed in the N_2 flux. This indicates that the average crossing pore size is smaller than 0.2 μm, in good keeping with the known particle size (0.33 μm) of the alumina raw material used to prepare the fibre.

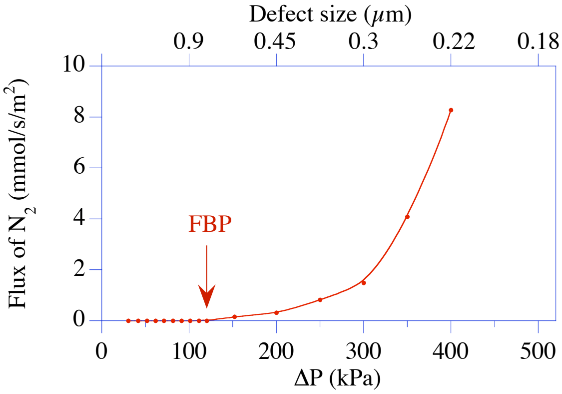

Fig. 2. Variation of N_2 flow through an ethanol soaked fibre support (FBP, First Bubble Point)

3.2. *Physical characterisations*

Weight uptake & elemental analysis

The weight measurement just after synthesis and calcination provided a direct uptake of ca. 10% of the fibre mass.

Elemental analysis of the fibre showed no Si in the fibre before zeolite synthesis, and 51.5 ± 0.3 wt.%. of Al (close to the theoretical 52.9 wt.% of Al_2O_3). After synthesis, the Si and Al compositions were, respectively, 4-5 and 44-46 wt.%.

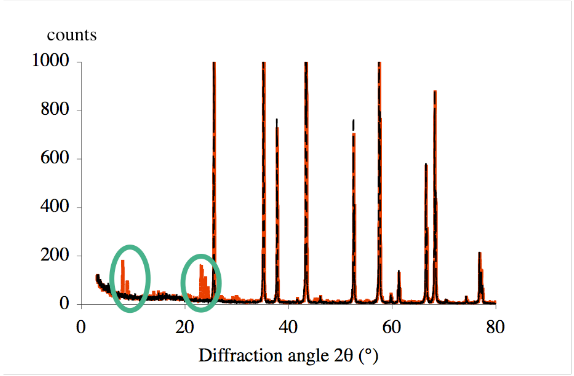

Fig. 3. XRD patterns of a fibre before (black line) and after (red line) zeolite synthesis. The circles refer to peaks related to the MFI phase.

X-ray Diffraction

Fig. 3 shows the XRD pattern of a crushed fibre before and after zeolite synthesis and calcination. As can be seen, pure MFI was the only zeolitic phase on the fibre after synthesis, without evidence of a significant presence of amorphous silica.

Macroporosity

Fig. 4 shows the evolution of macroporosity, as measured by mercury porosimetry. Note that considering the small mass of both samples, these measurements should be regarded as indicative. However, one can see that the total porosity (for pores between 0.01 and 400 μm) of the sample was reduced from about 43% before zeolite synthesis down to about 24% just afterwards. Moreover, after synthesis, the pore size distribution is shifted towards smaller pores, from an important contribution centred between 0.26 and 0.46 μm to a bit less than 0.1 μm. Please note that (i) the mass of sample is limited and (ii) the pores observed here can be crossing as well as dead-end pores. Therefore, no qualitative conclusion can be driven from the derivative curves.

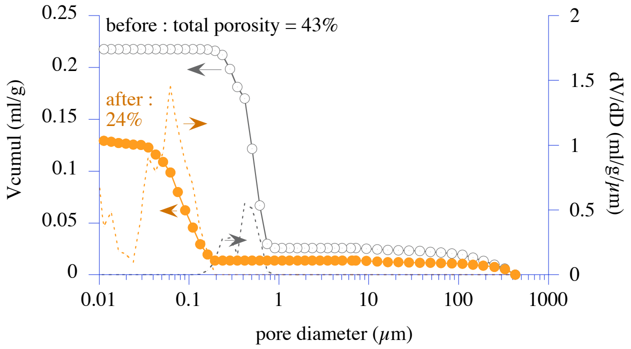

Fig. 4. Cumulated (left axis) and derivative (right axis) volumes as a function of pore diameter obtained from mercury porosimetry. Open symbols: support fibre, full symbols: zeolite – alumina fibre.

Microporosity

Fig. 5 shows the N_2 adsorption isotherm at 77 K on crushed fibres before and after zeolite synthesis. The N_2 isotherm after synthesis shows a rapid N_2 uptake at low P/P^0 ratios, followed by a plateau typical of a Type I isotherm. Moreover, the N_2 adsorption loadings are ca. 7 times higher after zeolite synthesis than for the fresh fibres.

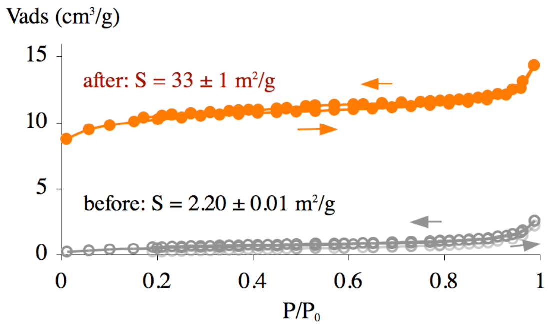

Fig. 5. N_2 adsorption/desorption isotherms at 77 K of a fibre before (bottom) and after (top) zeolite synthesis.

Electron microscopy

Fig. 6 shows cross section SEM micrographs of the fibre before zeolite synthesis. The support exhibits very large pores or holes actually restricting the equivalent thickness to a fraction of the apparent wall thickness (about an order of magnitude, close to 20 μm). The higher magnification micrograph reveals a pore size of about 0.3-0.4 μm (bottom of Fig. 6) in an area located between the largest holes.

Fig. 7 shows similar views of the hollow fibre after zeolite synthesis in a growing magnification order. The views show both a part of the cross section of the fibre and some of its internal surface. The grains of the alumina support can be clearly identified, and no surface film of zeolite crystals can be observed, even at higher magnifications (bottom of Fig. 7). In this last view, crystalline features can be recognised, where before synthesis were located the support pores.

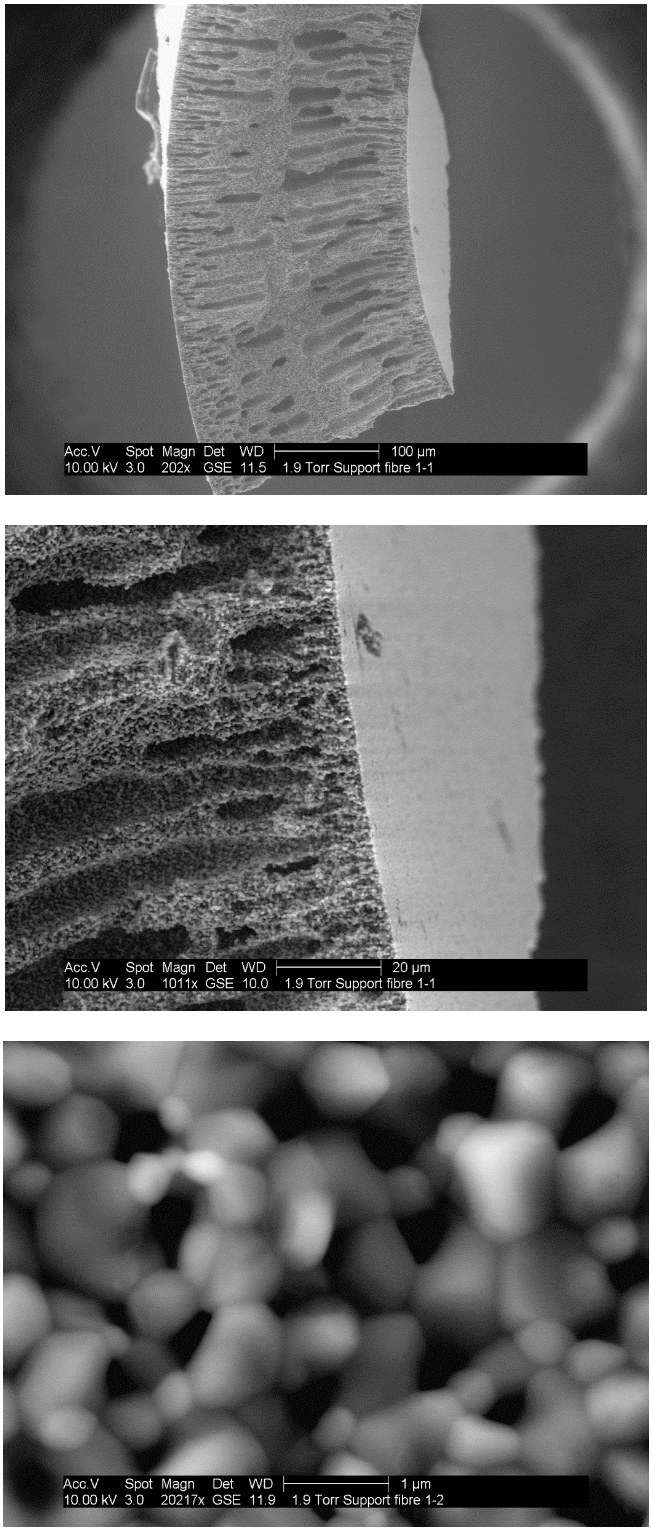

Fig. 6. SEM micrographs of the support hollow fibre before zeolite synthesis with increasing magnification from top to bottom.

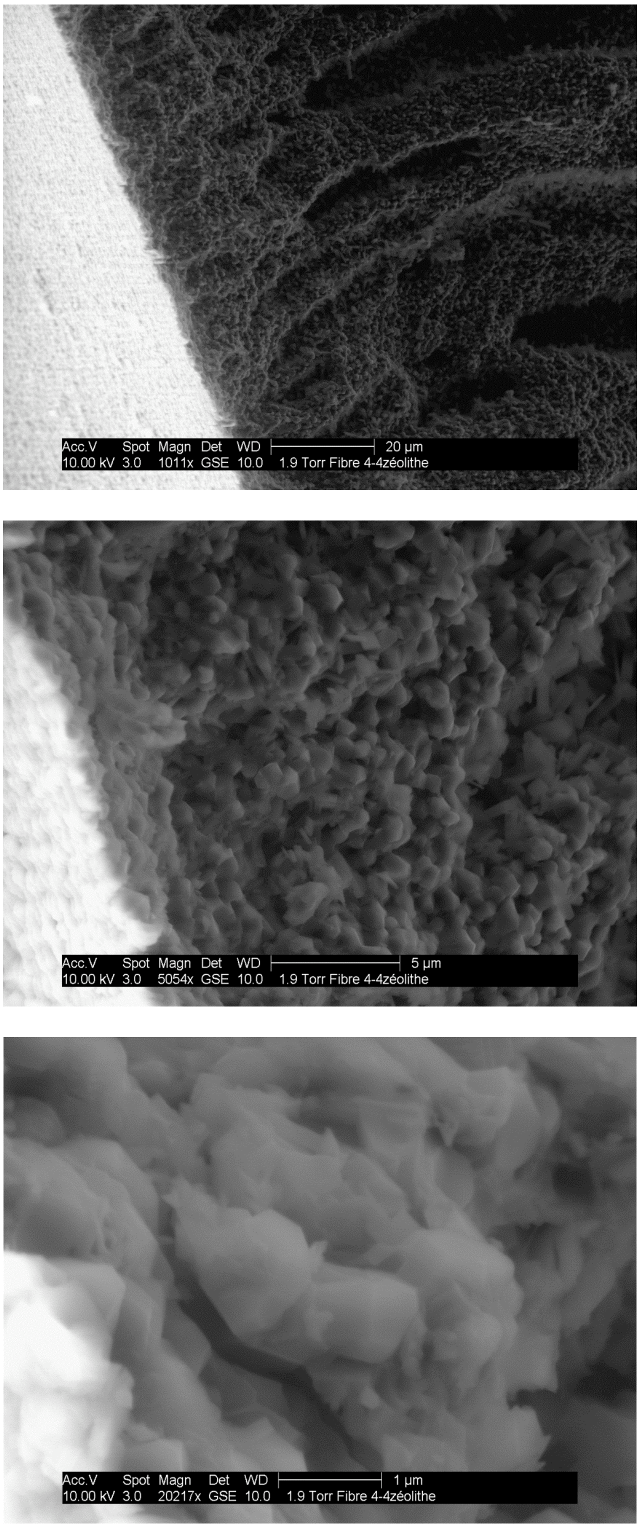

Fig. 7. SEM micrographs of the nanocomposite MFI-alumina hollow fibre membrane with increasing magnification from top to bottom.

Further EDX analyses were carried out on a large number of regions to investigate the material hosted in the α-alumina fibres after synthesis. As expected, the support exhibits only the presence of Al and O before synthesis, while after synthesis and calcination, the fibre shows significant amounts of Si (8-12 wt.%) on the cross section in homogeneous regions (i.e. out of the larger holes, those showing large amounts of disjoined large MFI crystals). Note that all these measurements were difficult to perform due to the heterogeneity of the cross section.

The Si concentration increases closer to the surface of the fibre wall. An outer surface EDX measurement provided similar values for the Si loading (up to 13 wt.% in average). However, patches of higher concentration areas (i.e. pieces of pure MFI crystals) have been found on some places on the surface.

3.3. H_2 and N_2 permeance

A first series of tests were carried out using single gas permeation experiments for N_2 at room temperature after *in-situ* thermal treatment at 673 K for 4 h. The permeance of fibre supports, before zeolite synthesis, was about 50 μmol·m^{-2}·s^{-1}·Pa^{-1} at 1.0 bar average pressure, which is of the same order to that of single three layered 200-nm α-alumina tubes used in previous works to synthesise nanocomposite MFI-type membranes [8]. On nanocomposite MFI/alumina fibres, the permeance was reduced to about 1 μmol·m^{-2}·s^{-1}·Pa^{-1}.

Fig. 8 shows the variation of H_2 and N_2 single gas permeance through a nanocomposite MFI/alumina fibre samples as a function of temperature, together with the Maxwell-Stefan (MS) fittings according to the following expression:

$$N = \frac{c_{sat}\rho\varepsilon D_o^{\infty}}{\tau\ell}\ln\left[\frac{1+\dfrac{P_R}{P^o}\exp\left(\dfrac{\Delta S^o_{ads}-R}{R}-\dfrac{\Delta H^o_{ads}}{RT}\right)}{1+\dfrac{P_P}{P^o}\exp\left(\dfrac{\Delta S^o_{ads}-R}{R}-\dfrac{\Delta H^o_{ads}}{RT}\right)}\right]\exp\left[-\frac{E_D}{RT}\right] \qquad (2)$$

with (parameter values taken from [5]):

- R: ideal gas constant (8.314 J·mol^{-1}·K^{-1})
- c_{sat}: concentration of the gas in MFI crystals (5.4 mol·m^{-3} for both gases)
- ρ_{MFI}: density of MFI (1700 kg·m^{-3})
- ε: porosity of the nanocomposite MFI / alumina structure (0.13)
- D_0^{∞}: Maxwell-Stefan diffusivity at zero coverage (H_2: 1.8·10^{-8} m^2·s^{-1}, N_2: 0.4·10^{-8} m^2·s^{-1})
- τ: tortuosity (1.2)
- ℓ: equivalent MFI thickness (m, fitted parameter)
- P_R: retentate pressure [Pa]
- P_P: permeate pressure [Pa]
- P^o: reference to atmospheric pressure (101325 Pa)
- ΔS^o_{ads}: standard adsorption entropy (H_2: -43, N_2: -50 J·mol^{-1}·K^{-1})
- ΔH^o_{ads}: standard adsorption enthalpy (H_2: -5900 J·mol^{-1}, N_2: -13800 J·mol^{-1})
- E_D: diffusion activation energy (H_2: 2000 J·mol^{-1}, N_2: 4000 J·mol^{-1})

As can be seen, the permeance of both gases shows a continuous decrease with temperature. The MS fittings reflect an equivalent MFI thickness close to 1 μm. Note that the observed variations show no indication of permeance increase at higher temperature up to 723 K.

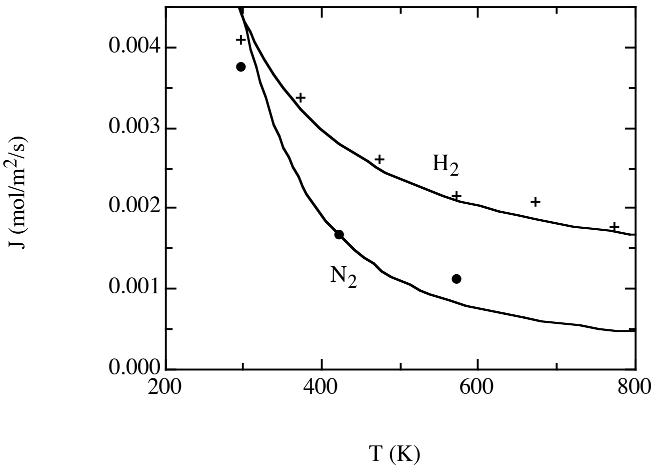

Fig. 8. Evolution of single gas permeance of H_2 (+) and N_2 (•) through a nanocomposite MFI/alumina fibre. Conditions: retentate pressure 105 to 125 kPa and transfibre pressure 3.2 kPa. The line corresponds to the fitting to the MS model (Eq. 2).

3.4. Separation of butane/H_2 and CO_2/H_2 mixtures

Fig. 9 shows the performance of two nanocomposite MFI/alumina fibre towards separation of butane/H_2 equimolar mixtures on the same fibre sample than on Fig. 8, together with a similar result obtain on another sample.

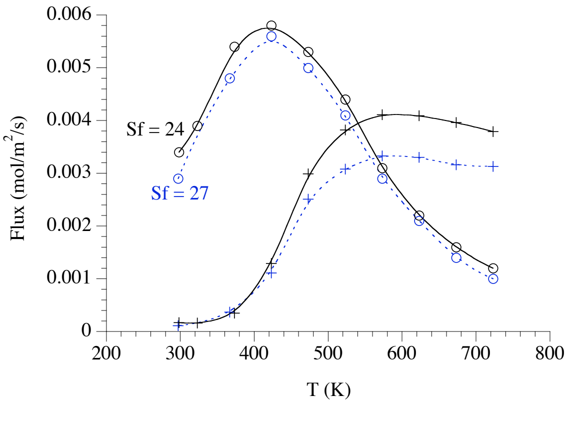

Fig. 9. Evolution of gas flux of butane and H_2 during butane/H_2 separation with temperature in an equimolar mixture through two nanocomposite MFI/alumina fibres (full and dotted lines) after pretreatment at 673 K for 4 h. Symbols: (o), butane flux; (+), hydrogen flux. Conditions: retentate pressure 125 kPa and transfibre pressure 0.4 kPa. Lines are guides to the eye.

The molar flux of both gases is shown as a function of temperature, from 300 to 723 K. Note that for both gases, the molar flux shows a decreasing trend at higher temperature. The separation factors (Sf) in favour of butane at low temperature are 24 and 27.

Fig. 10 shows the separation of CO_2/H_2 equimolar mixtures at room temperature as a function of the average pressure. As can be seen, the fibres synthesized in this work show CO_2/H_2 separation factors up to 10 at 180 kPa average pressure and room temperature. The CO_2 mixture permeances reach the value 0.12 $\mu mol \cdot m^{-2} \cdot s^{-1} \cdot Pa^{-1}$ at 100 kPa at room temperature.

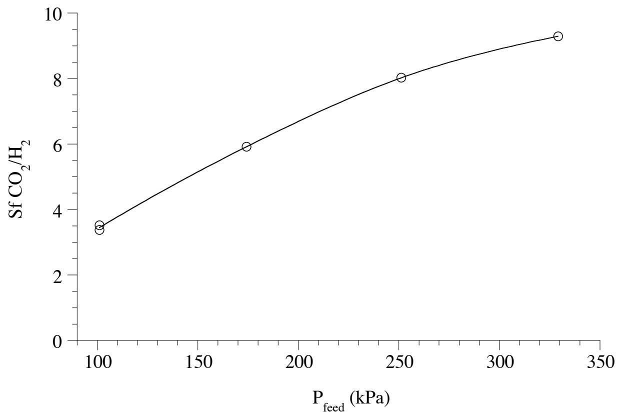

Fig. 10. Evolution of CO_2/H_2 separation factor with feed pressure in an equimolar mixture through a nanocomposite MFI/alumina fibre after pre-treatment at 673 K for 4 h. Conditions: temperature 300 K transfibre pressure 700 Pa. The line is a guide to the eye.

4. Discussion

4.1. MFI growth

The weight uptake directly measured after calcination (~100 mg MFI / g support) agrees fairly well with the values that can be computed from support macroporosity reduction, BET specific surface increase and Si/Al ratios obtained after MFI synthesis. First, the macroporosity of the support, as determined from Hg porosimetry (see Fig. 5) shows a cumulative pore volume decrease of about 40%, corresponding to about 0.09 cm^3/g. This reduction would correspond to a deposition of 113 mg MFI / g support taking a MFI density of 1.7 g/cm^3 and a microporosity of 30% (apparent density 1.2 g/cm^3). This is in fairly good agreement with the values obtained from direct weight uptake measurement.

Second, the BET surface area of a crushed fibre shows an increase of $33 - 2.2 = 30.8$ m^2/g after synthesis. If we consider a BET surface area in the order of 1000 m^2/g for MFI, as determined in our premises from pure MFI powder deposited at the bottom of the autoclave after synthesis, the computed weight uptake is about 110 mg MFI / g support. This value also matches the values obtained from direct weight uptake measurement and support macroporosity reduction. Moreover, the form of the N_2 adsorption/desorption curves on the crushed fibres after synthesis approaches a Type I isotherm, as expected for a material highly enriched in MFI microporous material.

Third, all these computed excesses are also similar to that deduced from Si concentration (4-5 wt.%, i.e. ≈10%wt. SiO_2) measured by elemental (ICP) analysis. Taking. The EDX analysis provide numbers in the same order of magnitude, but are much less precise.

Finally, in light of the results obtained from MS fittings to H_2 permeation, the equivalent MFI thickness to permeation (1 μm) accounts for a very low proportion of the total weight of the synthesized MFI material (about one hundredth). The remaining material should therefore be attributed to zeolite crystals blocking partially fibre macropores, but badly intergrown. This result reinforces the idea that most of the zeolitic material contributes only to a certain extent to pore-plugging, as can be inferred from the reduction of the mean pore size of the fibres from 0.46 to 0.26 μm provided by Hg porosimetry.

4.2. Nanocomposite nature of MFI/alumina fibres

The SEM micrographs (Figs. 6 and 7) reveal that no film is formed on the top of the support. This has been confirmed by a local EDX analysis of the top view. In this zone, the Si concentration is similar to that observed on the bare fibre. In these zones, the Si/Al ratio is fairly constant over the thickness of the material. Taking into account the relative density of the host ceramic and that of MFI, as well as the porosity of the fibres (43%), the ratio observed (0.1-0.2) indicates an important proportion of pores filled by the zeolitic material, as expected for a nanocomposite membrane structure [6].

4.3. Fibre quality

Before calcination, no significant N_2 permeance was observed due to the presence of the structure directing agent blocking the zeolite pores. This result shows that only one synthesis cycle should be enough to build a defect-free membrane.

This is confirmed by the high n-butane / hydrogen separation factors obtained at low temperature, when compared to previous studies on conventional single tubes [5].

4.4. Thermal behaviour of single gas permeance

The absolute permeance values of H_2 and N_2 through the MFI/alumina fibres at room temperature (see Fig. 8) are close to those found in MFI membranes [5,11,13]. This result is opposite to the idea put forward by some authors [14] that embedding the zeolite crystals into the support pores may lead to lower permeance values. In this case, the synthesis of very thin intergrown MFI nanocomposites in the macroporosity of the support, with equivalent thickness close to 1 μm, as computed from MS modelling, prevents the membranes from a sharp reduction of gas permeance.

Moreover, pure H_2 and N_2 fluxes show a continuous decrease with temperature in the range 273-723 K, in a similar manner as that found for nanocomposite

MFI/alumina tubular membranes [5]. This trend differs from that usually found in film-like MFI membranes (silicalite-1 and ZSM-5) grown on alumina and stainless steel supports, where H_2 and N_2 fluxes show a sharp increase over 400 K [11,13-17]. In the case of permeation of light hydrocarbons [17-21] and isobutene [22] within film-like MFI membranes, this flux increase at higher temperatures is observed after passing though a maximum, in keeping with adsorption.

Therefore, pure H_2 and N_2 fluxes within the nanocomposite MFI/alumina fibres synthesized in this work can be well described by the MS equation (Eq. 2), with no need to add an ‘activated diffusion’ term to account for flux increase at higher temperatures [20,23]. This discrepancy between both configurations has been attributed to the reversible opening of intercrystalline pathways in films upon heating owing to the negative expansion coefficients of the MFI structure [5], something that is not allowed in the nanocomposite architecture.

4.5. Gas separation

The n-butane/H_2 separation data presented in Fig. 10 are in excellent agreement with those experimentally determined by our group on nanocomposite MFI/alumina membranes [5]. Butane shows a maximum ca. 430 K and the n-butane/H_2 separation factor shows a decreasing trend with temperature from a value of 27 at room temperature to 0.3 at 723 K. However, in the case of fibres, the pure gas permeance is ca. 3 times higher than those that are obtained through MFI tubular membranes. This difference might be attributed to a lower MFI thickness (equivalent) in the former case, as computed from fittings of nitrogen and hydrogen permeance data to the MS model (1 μm in fibres vs. 3 μm in tubular membranes for the same fitting parameters).

Moreover, as observed for nanocomposite MFI/alumina tubular membranes, MFI/alumina fibres do not show a flux increase for both gases at higher temperatures [5]. Note that this trend is opposite to that reported by Kapteijn et al. [11] and many others on film-like MFI membranes, where n-butane and H_2 fluxes show a sharp increase over 500 K. Such increase at higher temperatures has also been observed in the separation of xylene mixtures within film-like MFI membranes grown on porous α-alumina and stainless steel supports, for which numerous results are available in the literature [24-28]. In the case of p-xylene, flux increase is observed above 480-573 K.

Finally, the results plotted in Fig. 10 reveal that the nanocomposite MFI/alumina fibres prepared in this work are promising candidates for CO_2 separation. The separation factors obtained in this work (up to 10) are of the same order to those that can be achieved using film-like MFI-type zeolite membranes at similar experimental conditions [9, 29-32]. However, these fibres offer higher permeances as well as much higher module surface / volume ratios.

5. Conclusion

Nanocomposite MFI/alumina hollow fibres with a negligible amount of intercrystalline defects and high gas permeance at room temperature have been successfully synthesized using the pore-plugging approach. In this nanocomposite architecture, grain boundaries that could limit selectivity are less important than in film-like structures.

The results presented in this work open up a new research line to scale up the fibre preparation process as an aim to obtain fibre bundles easy to scale-up to carry out separations of industrial interest, in particular CO_2 from flue gases. The advantage of such systems do not only arises from its nanocomposite nature, which allows selective separations at high temperature, but also on their very high surface/volume ratios when compared to conventional tubular MFI membranes (even of multichannel forms). The use of such systems might allow a reduction in size and cost of the permeating module. In turn, this might allow the development of technological solutions for CO_2 removal in numerous processes.

Acknowledgements

The Libyan embassy in Paris is greatly acknowledged for A. Alshebani’s grant. M. Pera-Titus grant is part of the European Marie-Curie Program (project # 041297). Abdeslam El Mansouri, of the European Institute for Membranes, is kindly acknowledged for the results of the mercury macroporosimeter. The authors are grateful to Prof. Joan Llorens, from University of Barcelona for helping with the low-temperature glaze.

References

[1] S. Husain, W.J. Koros, Mixed matrix hollow fiber membranes made with modified HSSZ-13 zeolite in polyetherimide polymer matrix for gas separation, J. Membr. Sci. 288 (2007) 195.

[2] S.P.J. Smith, V.M. Linkov, R.D. Sanderson, L.F. Petrik, C.T. O’Connor, K. Keiser, Preparation of hollow-fibre composite carbon-zeolite membranes, Micropor. Mater. 4 (1995) 385.

[3] H. Richter, I. Voigt, G. Fischer, P. Puhlfürβ, Preparation of zeolite membranes on the inner surface of ceramic tubes and capillaries, Sep. Purif. Technol. 32 (2003) 133.

[4] X. Xu, W. Yang, J. Liu, L. Lin, N. Stroh, H. Brunner, Synthesis of NaA zeolite membrane on a ceramic hollow fiber, J. Membr. Sci. 229 (2004) 81.

[5] S. Miachon, I. Kumakiri, P. Ciavarella, L. van Dyk, K. Fiaty, Y. Schuurman, J.-A. Dalmon, Nanocomposite MFI-alumina membranes via pore-plugging synthesis: Specific transport and separation properties, J. Membr. Sci. 298 (2007) 71.

[6] S. Miachon, E. Landrivon, M. Aouine, Y. Sun, I. Kumakiri, Y. Li, O. Pachtová Prokopová, N. Guilhaume, A. Giroir-Fendler, H. Mozzanega, J.-A. Dalmon, Nanocomposite MFI-alumina membranes via pore-plugging synthesis. Preparation and morphological characterisation, J. Membr. Sci. 281 (2006) 228.

[7] L. van Dyk, L. Lorenzen, S. Miachon, J.-A. Dalmon, Xylene isomerization in an extractor type Catalytic Membrane Reactor, Catal. Today 104 (2005) 274.

[8] P. Ciavarella, H. Moueddeb, S. Miachon, K. Fiaty, J.-A. Dalmon, Experimental study and numerical simulation of hydrogen/isobutane permeation and separation using MFI-zeolite membrane reactor, Catal. Today 56 (2000) 253.

[9] V. Sebastián, I. Kumakiri, R. Bredesen, M. Menéndez, Zeolite membrane for CO_2 removal: operating at high pressure, J. Membr. Sci. 292 (2007) 92.

[10] A. Goldbach, T. Mauer, N. Stroh, Keramische Hohlfaser- und Kapillamembranen, Keram. Z. 53 (2001) 1012.

[11] F. Kapteijn, W.J.W. Bakker, L.J.P. J.M. van der Graaf, G. Zheng, J. Poppe, J.A. Moulijn, Permeation behaviour of a silicalite-1 membrane, Catal. Today 25 (1995) 213.

[12] O. Pachtová, I. Kumakiri, M. Kocirik, S. Miachon, J.A. Dalmon, Dynamic desorption of adsorbing species under cross membrane pressure difference: a new defect characterisation approach in zeolite membranes, J. Membr. Sci. 226 (2003) 101.

[13] C. Bai, M. Jia, J.L. Falconer, R.D. Noble, Preparation and separation properties of silicalite composite membranes, J. Membr. Sci. 105 (1995) 79.

[14] J. Hedlund, F. Jareman, A.-J. Bons, M. Anthonis, A masking technique for high quality MFI membranes, J. Membr. Sci. 222 (2003) 163.

[15] K. Aoki, V.A. Tuan, J.L. Falconer, R.D. Noble, Gas permeation properties of ion-exchanged ZSM-5 zeolite membranes, Micropor. Mesopor. Mater. 39 (2000) 485.

[16] C.L. Flanders, V.A. Tuan, R.D. Noble, J.L. Falconer, Separation of C6 isomers by vapor permeation and pervaporation through ZSM-5 membranes, J. Membr. Sci. 176 (2000) 43.

[17] J. Coronas, J.L. Falconer, R.D. Noble, Characterization permeation properties of ZSM-5 tubular membranes, AIChE J. 43 (1997) 1797.

[18] M.P. Bernal, E. Piera, J. Coronas, M. Menéndez, J. Santamaría, Mordenite and ZSM-5 hydrophilic tubular membranes for the separation of gas phase mixtures, Catal. Today 56 (2000) 221.

[19] F. Kapteijn, J.M. van der Graaf, J.A. Moulijn, One-component permeation maximum: diagnostic tool for silicalite-1 membranes?, AIChE J. 46 (2000) 1096.

[20] W.J.W. Bakker, L.J.P. van den Broeke, F. Kapteijn, J.A. Moulijn, Temperature dependence of one-component permeation through a silicalite-1 membrane, AIChE J. 43 (1997) 2203.

[21] W.J.W. Bakker, F. Kapteijn, J.Poppe, J.A. Moulijn, Permeation characteristics of a metal-supported silicalite-1 zeolite membrane, J. Membr. Sci. 117 (1996) 57.

[22] G. Li, E. Kikuchi, M. Matsukata, ZSM-5 zeolite membranes prepared from a clear template-free solution, Micropor. Mesopor. Mater. 60 (2003) 225.

[23] A.J. Burggraaf, Single gas permeation of thin zeolite (MFI) membranes: theory and analysis of experimental observations, J. Membr. Sci. 155 (1999) 45.

[24] A.M. Tarditi, S. Irusta, E.A. Lombardo, Xylene isomerization in a membrane reactor. Part I: The synthesis of MFI membranes for the p-xylene separation, Chem. Eng. J. 122 (2006) 167.

[25] C.J. Gump, V.A. Tuan, R.D. Noble, J.L. Falconer, Aromatic permeation through crystalline molecular sieve membrane, Ind. Eng. Chem. Res. 40 (2001) 565.

[26] G. Xomeritakis, Z. Lai, M. Tsapatsis, Separation of xylene isomer vapors with oriented MFI membranes made by seeded growth, Ind. Eng. Chem. Res. 40 (2001) 544.

[27] Z. Lai, M. Tsapatsis, Gas and organic vapor permeation through b-oriented MFI membranes, Ind. Eng. Chem. Res. 43 (2004) 3000.

[28] X. Gu, J. Dong, T.M. Nenoff, D.E. Ozokwelu, Separation of p-xylene from multicomponent vapour mixtures using tubular MFI zeolite membranes, J. Membr. Sci. 280 (2006) 624-33.

[29] M.P. Bernal, J. Coronas, M. Menéndez, J. Santamaría, Separation of CO_2/N_2 mixtures using MFI-type zeolite membranes, AIChE J. 50 (2004) 127.

[30] S.H, Hyun, J.K. Song, B.I. Kwak, J.H. Kim, S.A. Hong, Synthesis of ZSM-5 zeolite composite membranes for CO2 separation, J. Mater. Sci. 34 (1999) 3095.

[31] H. Guo, G. Zhu, H. Li, X. Zou, X. Yin, W. Yang, Sh. Qiu, R. Xu, Hierarchical growth of large-scale ordered zeolite silicalite-1 membranes with high permeability and selectivity for recycling CO_2. Angewandte Chemie Int. Ed. 45 (2006) 7053.

[32] M.C. Lovallo, A. Gouzinis, M. Tsapatsis, Synthesis and characterization of oriented MFI membranes prepared by secondary growth, AIChE J. 44 (1998) 1903.